Published in final edited form as:
Structure. 2010 November 10; 18(11): 1492–1501. doi:10.1016/j.str.2010.08.012.

Structure and Flexibility of the Complete Periplasmic Domain of BamA. The Protein Insertion Machine of the Outer Membrane

Petia Zvezdanova Gatzeva-Topalova, **Lisa Rosa Warner**, **Arthur Pardi**, and **Marcelo Carlos Sousa**
Department of Chemistry and Biochemistry, University of Colorado at Boulder, Boulder, CO 80309, USA

Summary

Folding and insertion of β-barrel outer membrane proteins (OMPs) is essential for Gram-negative bacteria. This process is mediated by the multiprotein complex BAM, composed of the essential β-barrel OMP BamA and four lipoproteins (BamBCDE). The periplasmic domain of BamA is key for its function and contains five “polypeptide transport-associated” (POTRA) repeats. Here we report the crystal structure of the POTRA4-5 tandem, containing the essential for BAM complex formation and cell viability POTRA5. The domain orientation observed in the crystal is validated by solution NMR and SAXS. Using previously determined structures of BamA POTRA1-4 we present a spliced model of the entire BamA periplasmic domain validated by SAXS. Solution scattering shows that conformational flexibility between POTRA2 and 3 gives rise to compact and extended conformations. The length of BamA in its extended conformation suggests that the protein may bridge the inner and outer membranes across the periplasmic space.

INTRODUCTION

The outer membrane (OM) of gram-negative bacteria consists of lipopolysaccharide, phospholipids and outer membrane proteins (OMPs). These OMPs have a characteristic β-barrel structure embedded in the outer membrane (Schulz, 2003). The correct folding and insertion of β-barrels into the OM are essential for bacteria. However, the mechanisms mediating these processes are not well understood. Several key players involved in the OMP biogenesis have been identified (Malinverni et al., 2006; Sklar et al., 2007b; Voulhoux et al., 2003; Voulhoux and Tommassen, 2004; Wu et al., 2005) including a multi-protein complex in the outer membrane known as BAM (for **b**eta-barrel **a**ssembly **m**achine). This complex is anchored by BamA, a β-barrel OMP itself formerly known as YaeT in *E. coli*, and four lipoproteins: BamB (YfgL), BamC (NlpB), BamD (YfiO) and BamE (SmpA). BamA and BamD, are essential for cell viability and their depletion leads to accumulation of unfolded OMP aggregates in the periplasm and ultimately, cell death (Voulhoux et al., 2003; Wu et al., 2005). Null mutants of BamB, BamC and BamE are tolerated but result in OM defects and triggering of stress responses (Malinverni et al., 2006; Voulhoux et al., 2003; Wu et al., 2005).

Corresponding Contact: Marcelo C. Sousa, Telephone: 303 735 4341, Fax: 303 492 5894, Marcelo.Sousa@colorado.edu.

BamA belongs to the Omp85 family of proteins and is found in all Gram-negative bacteria. It contains an N-terminal periplasmic domain with five polypeptide transport-associated (POTRA) repeats in addition to the outer membrane-embedded C-terminal β-barrel domain (Gentle et al., 2005). The POTRA repeats are thought to mediate protein-protein interactions, nucleate β-strands formation in nascent OMPs and have chaperone-like activity (Habib et al., 2007; Hodak et al., 2006; Knowles et al., 2008; Sanchez-Pulido et al., 2003). Kim et al. tested the effects of deleting individual POTRA domains in *E. coli* BamA (Kim et al., 2007). The analysis revealed that POTRA1 or POTRA2 deletion mutants survive but grow poorly. In contrast, deletions of POTRA3, 4 or 5 result in loss of cell viability. Moreover, loss of POTRA5 results in disassembly of the BAM complex. Similar studies in *Neisseria meningitides* showed that only POTRA5 is essential in that bacterium (Bos et al., 2007).

Structures for the first four POTRA domains of BamA have been reported (Gatzeva-Topalova et al., 2008; Kim et al., 2007; Knowles et al., 2008). However, the structure of the essential POTRA5 and its conformation with respect to the other POTRA domains has remained unknown. Here we report the crystal structure of the POTRA4-5 tandem from *E. coli* BamA. NMR and Small Angle X-ray Scattering (SAXS) experiments show that the crystal structure is consistent with its conformation in solution. We also report a spliced model of the entire periplasmic domain of BamA derived from this structure and the previously reported structures of POTRA1-4. SAXS experiments validate the spliced model, and the conformational flexibility of the periplasmic domain of BamA is discussed.

RESULTS

Crystal Structure of *E. coli* BamA POTRA4-5

Crystal structures by Kahne and coworkers, as well as our lab, revealed two different conformations for the first four POTRA domains of BamA (Gatzeva-Topalova et al., 2008; Kim et al., 2007). However, these structures are missing the most C-terminal POTRA domain (POTRA5) that is essential for viability in both *E. coli* and *Neisseria meningitides* (Bos et al., 2007; Kim et al., 2007). Crystals of the entire periplasmic fragment of BamA containing all five POTRA domains diffracted poorly and were not amenable to structure determination. To determine the structure of the essential POTRA5 and its relative orientation with respect to the rest of the periplasmic domain, we crystallized the last two POTRA domains - POTRA4-5 ($BamA_{264-424}$). Crystals of the selenomethionine-substituted $BamA_{264-424}$ grew in 0.1M HEPES pH 7.5, 1.95-2.05M ammonium sulfate, 3% PEG 400, 0.15-0.25M NaCl; and a data set to 2.7Å at the selenium peak wavelength was collected from these crystals. The structure of $BamA_{264-424}$ was solved by MR-SAD techniques as described in Experimental Procedures. Data collection and refinement statistics are shown in Table 1.

BamA POTRA5 displays the characteristic POTRA structure with two α helices packaged against a mixed three-strand β sheet (Figure 1A, green). As previously reported (Gatzeva-Topalova et al., 2008; Kim et al., 2007), POTRA3 in *E. coli* BamA has several unique structural features such as a β-bulge in β2 and an extended L2 loop (yellow in Figure 1A), that set it apart from other POTRA domains. BamA POTRA5 does not display any of these features and has no significant structural differences with POTRA1, 2 or 4 (Figure 1A, POTRA5 superimposes on POTRA1 with root mean square deviation (RMSD) of 1.28Å over 67 Cα atoms). The only noticeable exception is a 3 amino acid deletion in L3 (Figure 1A, red) in both POTRA1 and POTRA5.

$BamA_{264-424}$ adopts an L-shaped conformation in the crystal (Figure 1B) with an angle of almost 90° between the two POTRA domains. The crystals contain two molecules in the

asymmetric unit (chains A and B). The interface between the two chains is relatively small (surface area of 1,154Å^2) stabilized by one salt bridge and few hydrogen bonds (Table S1) suggesting that dimerization is not biologically relevant. This is consistent with the protein behaving as a monomer in size exclusion chromatography (data not shown).

Chain A is well packed in the crystal lattice resulting in excellent electron density that allowed modeling of residues 262 to 421 with a refined average B factor of 29.1Å^2 for all protein atoms. Conversely, only a few lattice contacts stabilize the packing of chain B resulting in a model with an average B factor of 60.0Å^2 for all protein atoms. Loops 2 and 4 in POTRA4, and loop 1 in POTRA5 could not be modeled in chain B due to poor electron density. A superposition of the two chains reveals that the two molecules in the asymmetric unit have very similar conformations as reflected by an RMSD of 1.32Å for all Cα atoms (Figure 1B).

The two POTRA domains are bridged by a 3 amino acid linker ($G_{344}N_{345}R_{346}$, cyan, Figure 1C) and the interface is stabilized by several interactions (Figure 1C). The guanidinium group of R314 in POTRA4 makes a salt bridge with D383 and a hydrogen bond with S379 in POTRA5. Other inter-domain contacts include hydrogen bonds between main chain atoms of G313 and S379, G316 and F347, G316 and L377, as well as the hydroxyl group of Y319 and the carbonyl of T402. Interactions of R346 in the linker further stabilize the interface by simultaneously hydrogen bonding the carbonyl of Y315 in POTRA4 and forming a cation-π interaction with W376 in POTRA5. All of the above interactions are conserved in chain B except those of R314.

Since the periplasmic domain of BamA is a series of tandem POTRA repeats bridged by linkers, a certain amount of flexibility between domains is expected. However, the very similar conformation between the two chains in the asymmetric unit despite different packing environments, together with the conservation of the interface between domains, suggest that the POTRA4-5 structure is relatively rigid.

Solution NMR data is consistent with the crystal structure of BamA POTRA4-5

Solution NMR was used as an independent method for assessing the orientation of the two POTRA domains in BamA POTRA4-5. Residual dipolar couplings (RDCs) provide information on orientation of individual bond vectors in a molecule and can be used to determine the flexibility and relative orientation of rigid domains in a macromolecule (Bax et al., 2001; Fischer et al., 1999). The crystal structure coordinates for POTRA4 and POTRA5 were used to define two rigid domains connected by the 3 amino acid linker ($G_{344}N_{345}R_{346}$.) The backbone ^{1}H-^{15}N resonances were assigned using spectra obtained from traditional TROSY-based NMR pulse sequences and the automated assignment program PINE (Bahrami et al., 2009). Assignments were confirmed manually using NOESY-HSQC spectrum. The ^{1}H-^{15}N amide backbone RDCs were measured by analysis of 2D ^{1}H, ^{15}N IPAP HSQC spectra (Ding and Gronenborn, 2003) obtained under isotropic and partially aligned conditions (Bax et al., 2001). A total of 73 and 59 ^{1}H-^{15}N amide RDCs from POTRA4 and POTRA5, respectively, were measured.

The first step in a solution NMR domain orientation study is determination of the alignment tensors of the individual domains, using the crystal coordinates and the experimental RDCs for each domain (Fischer et al., 1999). The RDCs can then be predicted from the alignment tensors. Figure S1 shows a plot of the experimental and predicted RDCs for the individual POTRA4 and 5 domains. The ^{1}H-^{15}N RDCs are a sensitive function of the angle of the bond vector, so even slight differences in the orientations of the HN bond in the crystal and in solution leads to “structural noise” (Zweckstetter and Bax, 2002). Thus, only the subset of 70 RDCs that showed good agreement (within ± 5Hz) between the experimental and

predicted RDCs were used (Figure S1). The values for the rhombicity, R, and the magnitude of the principal component, D_a, of the alignment tensors for POTRA4 and 5 (Figure S1), were consistent with the two domains behaving as a single rigid species (Fischer et al., 1999). The next step is to determine the relative orientation of the two domains in an unbiased manner. To do this a pool of 100 structures with randomized orientations between the rigid POTRA4 and 5 domains was generated by varying the torsion angles in the 3-residue linker (Figure 2A). This pool of structures was subjected to constrained molecular dynamics calculations (Schwieters et al., 2006), where the experimental RDCs were included in the energy function as constraints and only the torsion angles in the linker were varied. The 20 lowest energy structures (average RMSD of 2.56Hz for all RDCs) are in good agreement with one another and with the crystal structure (average RMSD of 3.40Å to the crystal structure over 160 Cα) as shown in Figure 2B, further supporting that the crystal structure is a good representation of the domain orientation in solution and not a result of crystal lattice contacts.

The solution scattering data validates the crystal structure of BamA POTRA4-5

As an additional independent validation of the structure of BamA POTRA4-5, we collected solution SAXS data for this BamA fragment. Scattering data were scaled and averaged in PRIMUS (Konarev et al., 2003) (Figure 3A, red). The theoretical scattering curve for BamA POTRA4-5 was computed using the crystal structure coordinates for chain A with the program CRYSOL (Svergun et al., 1995). Superposition of the experimental and coordinate-derived scattering curves shows excellent agreement with χ^2=2.2 (Figure 3A), suggesting that the protein adopts a conformation in solution similar to that observed in the crystal structure.

We used an indirect Fourier transformation of the scattering curve, as implemented in the program GNOM (Semenyuk and Svergun, 1991), to obtain the distance distribution function, P(r), which represents the sum of the lengths of all interatomic vectors in the molecule. The P(r) function computed from the crystallographic coordinates also shows excellent agreement with the experimental P(r) (Figure 3B). A peak at ~20Å corresponds to intradomain distances whereas the shoulder at ~40Å corresponds to vectors between the two POTRA domains. The radii of gyration (R_g) computed from the experimental and theoretical P(r) functions are indistinguishable within experimental error (22.98±0.01 and 22.18±0.01Å respectively) further demonstrating that the solution structure of BamA POTRA4-5 is consistent with the crystal structure.

Ab initio shape reconstructions from the SAXS data were performed with the program GASBOR (Svergun et al., 2001), which employs simulated annealing routines to search for a chain-like assembly of “dummy” residues that fits the experimental scattering curve (Svergun et al., 2001). Fifteen independent calculations were performed, all yielding similar solutions, as judged by the normalized spatial discrepancy (NSD) value ρ_f =0.98±0.18 calculated with DAMAVER (Volkov and Svergun, 2003). As shown in Figure 3C the averaged *ab initio* molecular envelope closely resembles the crystallographic structure. Docking of the crystal structure into the molecular envelope with SUPCOMB (Kozin and Svergun, 2001), results in NSD value ρ_f=0.85, indicating an excellent fit to the *ab initio* calculated envelope.

Next, we used the ensemble optimization method (EOM) to further evaluate whether the POTRA4-5 fragment is flexible in solution (Bernado et al., 2007). A pool of 10,000 random conformations was generated by treating the POTRA domains as rigid bodies with a hinge point in the linker between them (between residues F347 and Y348). The pool of structures was then subjected to a genetic algorithm to select a subset that best fits the experimental data. The EOM selected a set of four structures with similar conformation (ρ =0.79±0.05)

and the goodness of fit to the scattering curve (χ^2=2.2) is no better than the fit to the single crystallographic structure. Analysis with increased number of conformers did not improve the fit and the R_g values of the selected structures are distributed in a single narrow peak spreading over only 4Å (Figure S3A), consistent with a rigid conformation (Bernado et al., 2007; Bernado et al., 2009).

Spliced model of the complete BamA periplasmic domain

The crystal structure of BamA POTRA1-4 has been solved in two distinct conformations (Gatzeva-Topalova et al., 2008; Kim et al., 2007), which differ in the bending around the linker bridging POTRA domains 2 and 3. The two structures represent a bent conformation (PDB 2QCZ) (Kim et al., 2007), and an extended conformation (PDB 3EFC) (Gatzeva-Topalova et al., 2008). We superimposed POTRA4 in BamA POTRA4-5 with the same domain in the POTRA1-4 structures to generate spliced models of the entire periplasmic domain of BamA (Figure 4). The POTRA4 domain is in essentially the same conformation in all structures superimposing with an RMSD of 0.62 (2QCZ) in the bent structure and 0.70Å (3EFC) in the extended structure.

The SAXS solution structure of BamA POTRA3-5 is consistent with the spliced model

Analysis of the BamA POTRA1-4 structures suggested that this fragment consisted of two relatively rigid arms formed by POTRA1-2 and POTRA3-4 with a hinge point in the linker between POTRA2 and 3 (Gatzeva-Topalova et al., 2008). As shown above, the structure of BamA POTRA4-5 is also relatively rigid. It then follows that the structure of BamA POTRA3-5 should be well ordered, without a great deal of flexibility. We tested this hypothesis by comparing solution SAXS data from BamA POTRA3-5 with the spliced model of the same fragment.

Theoretical scattering curves were calculated from the POTRA3-5 fragment of the spliced model, and compared to the experimental scattering curves. The experimental and coordinate-derived scattering curves are in good agreement, χ^2=2.2 (Figure 5A), validating the spliced model. Likewise, the P(r) functions obtained from the scattering curves are also in good agreement (Figure 5B), with indistinguishable experimental and calculated R_g values of 27.2±0.01 and 26.3±0.01Å respectively.

Fifteen independent *ab initio* structure calculations were averaged and filtered as described in Experimental Procedures. The resulting molecular envelope was superimposed on the spliced POTRA3-5 model yielding an NSD value (ρ_f) of 0.89, underscoring the agreement between the SAXS data and the spliced crystallographic models (Figure 5C).

EOM was used to investigate flexibility of the POTRA3-5 fragment. Two separate pools of 10,000 structures were generated: (1) two rigid bodies with a hinge point in the linker between POTRA3 and POTRA4 (between Q265 and Y266), and (2) two rigid bodies with a hinge point in the linker between POTRA4 and POTRA5 (between F347 and Y348). The two pools were independently subjected to EOM's genetic algorithm to select the subset of structures that best fits the scattering data. Both cases yielded similar results with χ^2 values of 1.7 and 1.6 for pools 1 and 2 respectively. The R_g of the selected structures clustered in a single peak in both cases (Figure S3B) consistent with a relatively rigid structure. The goodness of fit of the ensembles to the experimental scattering curve is only marginally better than that of the spliced model further indicating that the spliced model is a good representation of the structure of BamA POTRA3-5 in solution.

Conformational flexibility in the periplasmic domain of BamA

As mentioned above, two conformations have been described for the periplasmic domain of BamA (Gatzeva-Topalova et al., 2008; Kim et al., 2007). We collected SAXS data from a BamA POTRA1-5 fragment to test the fit of the spliced models in the bent and extended conformations to the solution structure. Figure 6A shows the BamA POTRA1-5 solution scattering curve (in black) together with scattering curves derived from the two spliced models. Neither of the individual models fits the experimental scattering data very well as judged by the χ^2 values of 5.7 and 12.2 respectively for the extended and bent conformations. Comparison of P(r) functions derived from the experimental scattering data and the two spliced models further illustrates that neither of the individual models fully represents the solution structure (Figure 6B).

We previously suggested that the BamA periplasmic domain displays significant conformational flexibility in the junction between POTRA domains 2 and 3 (Gatzeva-Topalova et al., 2008). The poor fit of individual structures to the SAXS data supports this hypothesis. We thus tested if a mixture of the two spliced models better represents the solution scattering. The program OLIGOMER (Konarev et al., 2003) was used to optimize the scattering contributions from the bent and extended conformations to maximize the fit to the experimental data. A mixture consisting of 74% extended and 26% bent conformations significantly improved the fit, χ^2 =2.7 (Figure 6C, green).

Given the apparent conformational flexibility, *ab initio* calculations would not be expected to converge to a single structure (or a family of closely related structures). Indeed, fifteen independent GASBOR runs resulted in different structures with a high NSD value, ρ_f =1.77, consistent with significant flexibility in the system.

Multiple conformations contributing to the scattering data is best analyzed using the ensemble optimization method (Bernado et al., 2007; Bernado et al., 2009). A pool of 10,000 structures was generated with two rigid bodies —POTRA1-2 and POTRA3-5— and a hinge point in the linker between POTRA2 and POTRA3 (between residues V173 and S174). The EOM genetic algorithm was then used to select up to 100 structures that best describe the scattering data. The process resulted in a good fit (χ^2 = 1.49) and, as expected, the selected structures are different from one another with an NSD value ρ_f=1.91±0.17. Interestingly, whereas the R_g distribution of the structures in the initial random pool is monomodal (black in Figure 6D), the distribution for the selected structures is bimodal (purple, Figure 6D) with a predominant peak at R_g=42.6Å consistent with an extended conformation, and a smaller peak at R_g=30.6Å consistent with a compact conformation. This suggests that the periplasmic domain of BamA adopts preferential conformations in solution—compact and extended—rather than sampling a large number of equally probable conformations around the hinge between POTRA domains 2 and 3. To rule out that this was due to biases in the initial pool, the calculations were repeated with three independent pools: (1) 10,000 structures generated from the bent spliced model and a hinge between residues V173 and S174; (2) 10,000 structures generated from the extended spliced model and the same hinge; and (3) 10,000 structures generated from the extended spliced model and a hinge four residues long (G172-A175). The R_g distributions of the structures selected from each of these pools were essentially the same (Figure S3C) indicating no bias from the initial pool composition. Finally, EOM calculations using three rigid bodies (POTRA1-2; POTRA3-4 and POTRA5) did not improve the fit to the scattering data (data not shown) indicating that the linker between POTRA2 and 3 is the main source of conformational flexibility in the periplasmic domain of BamA.

DISCUSSION

BamA is an essential component of the BAM complex required for the folding and insertion of outer membrane proteins into the OM (Malinverni et al., 2006; Sklar et al., 2007a; Voulhoux et al., 2003; Voulhoux and Tommassen, 2004; Wu et al., 2005). It belongs to the Omp85 family of proteins, which are characterized by a C-terminal β-barrel domain embedded in the membrane and an N-terminal domain containing one or more POTRA repeats (Gentle et al., 2005). In all γ-proteobacteria the N-terminal (periplasmic) domain of BamA consists of five POTRA repeats (Gentle et al., 2005; Voulhoux and Tommassen, 2004) that play an important role in recognition, docking, and folding of OMPs before their insertion in the outer membrane (Habib et al., 2007; Hodak et al., 2006; Knowles et al., 2008; Sanchez-Pulido et al., 2003).

The number of essential POTRA domains differs within γ-proteobacteria, but the most C-terminal POTRA5 domain connected to the β-barrel is always required (Bos et al., 2007; Kim et al., 2007). The results presented here reveal the structure of this essential POTRA5 domain and its conformation with respect to the rest of the POTRA repeats in the periplasmic domain of BamA.

POTRA5 is a canonical POTRA domain with no significant structural differences with the other POTRA domains in BamA, despite low sequence conservation. The crystal structure determined here shows that POTRA5 forms an angle of almost 90° with POTRA4. This domain orientation was independently confirmed by NMR analysis of RDCs as well as SAXS. The RDC data showed that individual POTRA4 and 5 domains have similar magnitudes of their alignment tensors (Figure S1). Thus, a single alignment tensor was used to find orientations of the two domains that fit well to the RDCs. The resulting ensemble of minimized structures has similar domain orientation to that of the crystal. Having similar magnitudes for the alignment tensor of individual domains normally provides strong evidence for rigidity in solution (Fischer et al., 1999). However, since the two domains are the same size, they could show similar alignment tensors even with extensive conformational flexibility in the linker. Thus, amide proton NOEs in the linker region were analyzed to further examine the similarity of the crystal and solution structures. Figure S2 shows the observed NH-NH NOEs for residues 343 to 349 mapped onto the crystal structure. The pattern of NOEs provides strong evidence that: 1) the backbone around the linker region is in a similar conformation in the crystal and in solution; and 2) this backbone is relatively rigid in solution. The NOE data rule out significant conformational flexibility of the backbone in the linker region. Backbone dynamics would reduce the intensities of these amide proton NOEs due to conformational averaging and increased flexibility would reduce the efficiency of spin-spin exchange that gives rise to the NOE. Thus, the size and patterns of the observed NH-NH NOEs strongly supports that the backbone in the linker is well ordered and is in a conformation similar to that in the crystal.

The POTRA4-5 SAXS scattering curve as well as the P(r) function and the *ab initio* calculated molecular envelope closely match those derived from the crystal structure. Together with the NMR, this provides a cross-validation that the solution and crystal structures are similar. A previous SAXS study of the POTRA1-5 fragment of BamA suggested that the POTRA5 domain folds sharply back towards POTRA4, resulting in a stacked arrangement of these two POTRA domains (Knowles et al., 2008). Our crystallographic, solution NMR and SAXS data are not compatible with this model.

The interface between POTRA4 and 5, albeit small, is well defined and stabilized by several interdomain interactions leading to a relatively rigid structure. This is evidenced by the small differences in domain orientation between the two independent molecules in the

crystallographic asymmetric unit as well as the experimental NH-NH NOEs observed in the linker region.

Conformational flexibility can be identified by EOM analysis of SAXS data. In this method, a protein is divided into two or more rigid bodies bridged by linker(s) and a large pool of random conformations is generated. A subset of structures that best fits the scattering data is then selected (Bernado et al., 2007; Bernado et al., 2009). EOM can easily distinguish between rigid and dynamic proteins on the basis of the conformational variability of the selected structures and their R_g distributions (Bernado et al., 2007; Bernado et al., 2009). Rigid proteins tend to have small structural variability, showing NSD values < 1.5, and single-peak R_g distributions a few angstroms wide, because the scattering data is well fit by a family of conformationally similar structures. In contrast, flexible systems are characterized by large NSD values and R_g distributions that spread over 20 or more angstroms. For the POTRA4-5 fragment the NSD of the selected structures was 0.79±0.05 and the R_g distribution about 4Å wide (Figure S3A), indicative of a rigid structure.

Superimposing POTRA4-5 onto the previously determined POTRA1-4 structures (Gatzeva-Topalova et al., 2008; Kim et al., 2007) we generated spliced models of the entire periplasmic domain of BamA. We predicted that the five POTRA domain fragment would behave as two rigid bodies—POTRA1-2 and POTRA3-5—bridged by a flexible linker.

Initial NMR studies of the POTRA1-2 tandem suggested, based on the lack of interdomain NOEs, that the link between these two repeats might be flexible (Knowles et al., 2008). However, a more recent study from the same group using PELDOR spectroscopy indicates that only a narrow distribution of conformations are sampled by these domains and that the interface between them is well defined (Ward et al., 2009). This is consistent with observations from the crystal structures of BamA, pointing to rigidity of the POTRA1-2 tandem (Gatzeva-Topalova et al., 2008).

Analysis of the SAXS data from BamA POTRA3-5 validates the spliced model and indicates that this fragment is rigid in solution. The scattering curve derived from the spliced model of POTRA3-5 agrees well with the experimental scattering and produces similarly shaped P(r) function. The unbiased *ab initio* calculation of a molecular envelope consistently converges to the U shaped conformation predicted by the spliced model. EOM analysis of the SAXS data revealed small structural variability and a narrow distribution of R_g values in the selected ensemble of structures fitting the solution scattering, consistent with a rigid conformation. Allowing flexibility between POTRA3 and 4, or between POTRA4 and 5 did not further improve the fit to the scattering data, highlighting the conformational rigidity of the POTRA3-5 fragment.

SAXS data collected on BamA POTRA1-5 support conformational flexibility in the linker between POTRA2 and 3, as predicted from our models. Neither the extended nor the bent conformations by themselves fit well with the solution scattering. However, a mixture of the extended and bent conformations results in a much better fit suggesting that multiple conformations are required to model the behavior of the protein in solution. Indeed, the EOM genetic algorithm selects multiple conformations for the POTRA1-5 fragment. We expected that the R_g values of the selected structures would be distributed in a single broad peak consistent with the protein sampling a large number of equally probable conformations. However, the R_g distribution is distinctly bimodal suggesting that BamA preferentially adopts extended (large R_g) and compact (small R_g) conformations. It is thus possible that the two crystal structures of the POTRA1-4 fragment represent two preferential states of BamA rather than two conformations of a completely flexible system that happened to be trapped in the crystal lattice.

The significance of the flexibility in the BamA periplasmic domain is unknown. One possibility is that the POTRA "arm" movements play a role in formation of β-hairpins in nascent OMPs, as previously suggested (Gatzeva-Topalova et al., 2008). In this model, POTRA domains nucleate β-strand formation in the substrate OMP (Gatzeva-Topalova et al., 2008; Kim et al., 2007) whereas transitions from extended to bent conformations in BamA might help create the turn, which is thought to be the rate-limiting step in the formation of β-hairpins (Du et al., 2004). Another possibility is that extended conformations of BamA permit the protein to bridge the inner and outer membranes. Such a model could allow the BAM complex to engage the SEC translocation machinery directly, establishing a trans-envelope assembly for transport of OMPs from the cytosol to the outer membrane. The length of the periplasmic domain of BamA in the extended conformation is approximately 105Å (Figure 7A), which is not much shorter than the thickness of the periplasm estimated to be 140Å (Collins et al., 2007; Graham et al., 1991). Moreover, the P(r) function computed from the POTRA1-5 SAXS data shows that the protein adopts solution conformations with interatomic distances of up to 140Å (Figure 6B). This suggests that the periplasmic domain of BamA may adopt conformations allowing the protein to bridge the inner and outer membranes. Focused experimentation is needed to test these hypotheses as well as the importance of BamA flexibility and its modulation by the lipoproteins of the BAM complex.

The results presented here provide a view of the structure and flexibility of the periplasmic domain of BamA. However, the conformation of this domain with respect to the transmembrane β-barrel is not known. FhaC is the only member of the Omp85 family for which the structure of both POTRA and β-barrel domains is known (Clantin et al., 2007). However, FhaC contains only two POTRA domains and shares limited sequence similarity with BamA. Moreover, BamA and FhaC are functionally distinct- FhaC is involved in the secretion of hemolysin-like polypeptides across the outer membrane rather than folding and insertion of OMPs. Therefore, models of BamA based on FhaC have to be analyzed carefully. Figure 7 shows the periplasmic domain of BamA superimposed on the FhaC structure including the β-barrel domain for reference. POTRA5 of BamA superimposes well with POTRA2 of FhaC (these are the POTRA domains closest to the β-barrel in both proteins) but the structures diverge at the link with the next POTRA domain. In FhaC the angle between POTRA1 and 2 is approximately 150°, whereas it is about 90° in BamA. It is possible that the conformation of the β-barrel and the adjacent POTRA domain in FhaC is retained in BamA. That case would result in the POTRA domains of BamA adopting a helical arrangement underneath the β-barrel domain (Figure 7). On the other hand, sequence alignment of the FhaC and BamA β-barrels indicate the presence of an insertion in BamA that maps to the loop potentially contacting POTRA5 (shown in red in Figure 7). This insertion makes it very difficult to develop homology models of the BamA β-barrel domain and understanding its conformation with respect to the periplasmic POTRA domains awaits structure determination.

EXPERIMENTAL PROCEDURES

Procedures for protein expression, purification and crystallization are detailed in the Supplemental Information.

Structure Determination and Refinement

Crystals of $BamA_{264-424}$ (POTRA4-5) belong to space group $P3_221$. Cell parameters are shown in Table 1. The self-rotation function showed 2-fold symmetry, which was incorporated in the locked cross rotation function of molecular replacement calculations using MOLREP (Vagin and Teplyakov, 2010), with SeMet data to 3.2Å resolution and the POTRA4 domain structure (Gatzeva-Topalova et al., 2008) (PDB ID 3EFC) as the search model.

Phases from the MR solution were combined with SAD phases in a PHENIX MRSAD job (Schuermann and Tanner, 2003). Initial phases were improved by density modification that led to readily interpretable maps, and allowed building of the POTRA5 domains in the both chains in the asymmetric unit using the program O (Jones, 1978). Iterative cycles of refinement in PHENIX (Adams et al., 2010) followed by manual rebuilding in O led to a significant decrease in R-values. Phases derived from the model were used to compute an anomalous difference Fourier map. Eight out of the ten methionines (five Met per copy including the N-terminal Met) in the two copies of POTRA4-5 coincided with anomalous difference peaks displaying sigma values larger then 3. The N-terminal methionine for copy B, as well as M325 did not show peaks in the anomalous difference Fourier map, and coincide with very flexible portions of the molecule, as judged by high B factor values. Cycles of refinement and rebuilding were continued until no further decrease in R-factors was observed. At this point, water molecules were added to the model. An additional round of refinement with TLS was performed in PHENIX, using each POTRA domain as a separate group. The final model contains residues 264-421 (plus 2 additional N-terminal residues resulting from the cloning) for copy A, and residues 264-420 for copy B. In several regions of copy B the electron density was not well defined, including residues G270-V271, I290-G293, P326-V335, D358-D362. Phasing and refinement statistics are summarized in Table 1.

Atomic coordinates and structure factors have been deposited in the PDB with accession number 3OG5.

Small Angle X-ray Scattering

Samples of $BamA_{21-424}$+6His (POTRA1-5), $BamA_{175-424}$ (POTRA3-5) and $BamA_{264-424}$ (POTRA4-5) were dialyzed overnight at 4°C against 25mM Tris pH8, 0.15M NaCl, 5% glycerol, and then filtered through 0.1μm filters. Data for POTRA4-5 were collected on Beamline 4-2 of the Stanford Synchrotron facility SSRL. Data for POTRA1-5 and POTRA3-5 were collected at beamline 12.3.1 of the Advanced Light Source (Lawrence Berkeley National Laboratory). Scattering data were collected at several protein concentrations and background scattering resulting from the buffer was subtracted. Initial analysis of the data, including scaling and averaging was performed using the program PRIMUS (Konarev et al., 2003). For POTRA4-5 several scattering data sets at 4mg/mL using 2s exposures were collected and combined, covering q ranges between 0.025 and 0.26 $Å^{-1}$. Data for POTRA3-5 collected using 5s exposures from samples at 1.2, 2.4 and 4.8 mg/mL were combined. For POTRA1-5, data using 1 and 5s exposures from samples at 1.35, 2.7 and 5.4 mg/mL were combined. Data for POTRA3-5 and POTRA1-5 covered q ranges between 0.04 and 0.27 $Å^{-1}$. P(r) functions were calculated using the program GNOM (Semenyuk and Svergun, 1991) with a maximum particle diameter of 80 Å for POTRA4-5, 85 Å for POTRA3-5, and 140 Å for POTRA1-5. Theoretical scattering curves were computed and compared to experimental scattering curves using the program CRYSOL (Svergun et al., 1995). In the case of POTRA1-5 two theoretical spliced models were evaluated for their relative contribution to the experimental scattering using the program OLIGOMER (Konarev et al., 2003). Flexibility of the system was investigated using EOM (Bernado et al., 2007; Bernado et al., 2009).

Ab initio calculations were performed with GASBOR (Svergun et al., 2001). Fifteen independent runs in GASBOR were performed for each, POTRA3-5 and POTRA4-5, and then the most probable model was computed with DAMAVER (Volkov and Svergun, 2003). Docking of the crystal structure of POTRA4-5, or the POTRA3-5 spliced model to the *ab initio* calculated envelope was performed with SUPCOMB (Kozin and Svergun, 2001).

NMR Backbone Assignments

The POTRA4-5 sample was concentrated to ~1 mM in NMR buffer [50 mM MES (pH 6.5), 50 mM NaCl, 0.1 mM EDTA, 0.01% NaN_3, 0.15 mM TSP, Complete EDTA-free protease inhibitor cocktail (Roche) 1 tablet/100 ml, 5% (V/V) D_2O]. NMR experiments for backbone assignments were collected using the TROSY-based Varian Biopack Suite: 2D ^{1}H, ^{15}N HSQC, 3D HNCACB, 3D CBCA(CO)NH and 3D NOESY-HSQC. Experiments were collected at 30°C on a VNMRS 800 MHz spectrometer equipped with a HCN z-axis gradient cold probe. Spectra were processed with NMRPipe (Delaglio et al., 1995) and analyzed with CCPNMR Analysis (Vranken et al., 2005). Peak lists from the ^{1}H, ^{15}N HSQC, HNCACB and CBCA(CO)NH spectra were used as input to the PINE server for automated assignment (Bahrami et al., 2009). Assignments were verified manually using backbone connectivities and NOEs in CCPNMR Analysis.

Measurement of Residual Dipolar Couplings and Domain Orientation

The amide ^{1}H-^{15}N RDCs were measured on a ~0.7 mM ^{15}N, ^{13}C-labeled POTRA4-5 sample (in NMR buffer with an additional 200 mM NaCl) in the presence and absence of ~8.8 mg/mL liquid crystalline Pf1 phage medium prepared as described (Hansen et al., 1998). Spectra were collected at 30°C on a Varian Inova 600 MHz spectrometer equipped with a HCN z-axis gradient cold probe. 2D HSQC HSQC sensitivity-enhanced ^{15}N-IPAP spectra (Ding and Gronenborn, 2003) were collected on the isotropic (no Pf1 phage) and aligned (with Pf1 phage) samples. The ^{1}H-^{15}N couplings were measured using CCPNMR Analysis (Vranken et al., 2005).

Molecular dynamics calculations were performed using the program XPLOR-NIH version 2.25. The magnitude and orientation of the alignment tensors for the individual POTRA domains were determined in XPLOR using the experimental RDCs and crystal coordinates. The two domains showed similar D_a and R (Figure S1), thus a single alignment tensor was used for the domain orientation calculations. A pool of 100 structures with random orientations for POTRA4 and 5 was generated starting with the crystal coordinates and performing a high temperature simulated annealing where only the torsion angles of the 3-amino acid linker ($G_{344}N_{345}R_{346}$) were varied. Each structure in the pool was subjected to simulated annealing torsion angle molecular dynamics calculations using a set of 75 ^{1}H-^{15}N amide RDCs that fit well (± 5 Hz) to the RDCs predicted from the individual domains (Figure S1). Two HN-HN NOE distance constraints (between residues 344-321 and 345-319) for the 3-residue linker region were included in the refinement to help position the domains. Only the torsion angles of the 3-residue linker were allowed to vary in the simulated annealing period and the POTRA4 and 5 domains were held rigid. The RDC (± 2.5 Hz) and NOE (ranges of 2.0 to 5.0 Å) constraints were included as pseudo-energy functions with a harmonic potential. The weighting of the RDCs was increased linearly and NOEs were held constant during the simulated annealing period. The set of lowest energy structures were used to represent the set of orientations for POTRA45 consistent with the RDC data.

HIGHLIGHTS

- BamA POTRA4-5 adopts an L shaped conformation.
- A spliced model of BamA POTRA1-5 is validated by SAXS.
- Conformational flexibility gives rise to bent and extended conformations.
- In the extended conformation BamA may bridge the inner and outer membranes.

Supplementary Material

Refer to Web version on PubMed Central for supplementary material.

Acknowledgments

This research was supported by NIH grant AI080709 to MCS; NIH training grant T32 GM08759 to LRW. Part of this work was performed at the Advanced Light Source, funded by the Department of Energy. The NMR instrumentation was purchased with partial support from NIH Grants RR11969 and RR16649, NSF Grants 9602941 and 0230966, and the W. M. Keck Foundation.

REFERENCES

Adams PD, Afonine PV, Bunkoczi G, Chen VB, Davis IW, Echols N, Headd JJ, Hung LW, Kapral GJ, Grosse-Kunstleve RW, et al. PHENIX: a comprehensive Python-based system for macromolecular structure solution. Acta Crystal Sect D. 2010; 66:213–221.

Bahrami A, Assadi AH, Markley JL, Eghbalnia HR. Probabilistic interaction network of evidence algorithm and its application to complete labeling of peak lists from protein NMR spectroscopy. PLoS Comput Biol. 2009; 5:e1000307. [PubMed: 19282963]

Bax A, Kontaxis G, Tjandra N. Dipolar couplings in macromolecular structure determination. Methods Enzym. 2001; 339:127–174.

Bernado P, Mylonas E, Petoukhov MV, Blackledge M, Svergun DI. Structural characterization of flexible proteins using small-angle X-ray scattering. J Am Chem Soc. 2007; 129:5656–5664. [PubMed: 17411046]

Bernado P, Perez Y, Blobel J, Fernandez-Recio J, Svergun DI, Pons M. Structural characterization of unphosphorylated STAT5a oligomerization equilibrium in solution by small-angle X-ray scattering. Protein Science. 2009; 18:716–726. [PubMed: 19309697]

Bos MP, Robert V, Tommassen J. Functioning of outer membrane protein assembly factor Omp85 requires a single POTRA domain. EMBO Rep. 2007; 8:1149–1154. [PubMed: 18007659]

Clantin B, Delattre AS, Rucktooa P, Saint N, Meli AC, Locht C, Jacob-Dubuisson F, Villeret V. Structure of the membrane protein FhaC: a member of the Omp85-TpsB transporter superfamily. Science. 2007; 317:957–961. [PubMed: 17702945]

Collins RF, Beis K, Dong C, Botting CH, McDonnell C, Ford RC, Clarke BR, Whitfield C, Naismith JH. The 3D structure of a periplasm-spanning platform required for assembly of group 1 capsular polysaccharides in Escherichia coli. Proc Natl Acad Sci U S A. 2007; 104:2390–2395. [PubMed: 17283336]

Delaglio F, Grzesiek S, Vuister GW, Zhu G, Pfeifer J, Bax A. Nmrpipe - a Multidimensional Spectral Processing System Based on Unix Pipes. J Biomol NMR. 1995; 6:277–293. [PubMed: 8520220]

Ding K, Gronenborn AM. Sensitivity-enhanced 2D IPAP, TROSY-anti-TROSY, and E.COSY experiments: alternatives for measuring dipolar 15N-1HN couplings. J Magn Reson. 2003; 163:208–214. [PubMed: 12914836]

Du D, Zhu Y, Huang CY, Gai F. Understanding the key factors that control the rate of beta-hairpin folding. Proc Natl Acad Sci U S A. 2004; 101:15915–15920. [PubMed: 15520391]

Fischer MW, Losonczi JA, Weaver JL, Prestegard JH. Domain orientation and dynamics in multidomain proteins from residual dipolar couplings. Biochemistry. 1999; 38:9013–9022. [PubMed: 10413474]

Gatzeva-Topalova PZ, Walton TA, Sousa MC. Crystal structure of YaeT: conformational flexibility and substrate recognition. Structure. 2008; 16:1873–1881. [PubMed: 19081063]

Gentle IE, Burri L, Lithgow T. Molecular architecture and function of the Omp85 family of proteins. Mol Microbiol. 2005; 58:1216–1225. [PubMed: 16313611]

Graham LL, Harris R, Villiger W, Beveridge TJ. Freeze-substitution of gram-negative eubacteria: general cell morphology and envelope profiles. J Bacteriol. 1991; 173:1623–1633. [PubMed: 1999383]

Habib SJ, Waizenegger T, Niewienda A, Paschen SA, Neupert W, Rapaport D. The N-terminal domain of Tob55 has a receptor-like function in the biogenesis of mitochondrial beta-barrel proteins. J Cell Biol. 2007; 176:77–88. [PubMed: 17190789]

Hansen MR, Mueller L, Pardi A. Tunable alignment of macromolecules by filamentous phage yields dipolar coupling interactions. Nature Struct Biol. 1998; 5:1065–1074. [PubMed: 9846877]

Hodak H, Clantin B, Willery E, Villeret V, Locht C, Jacob-Dubuisson F. Secretion signal of the filamentous haemagglutinin, a model two-partner secretion substrate. Mol Microbiol. 2006; 61:368–382. [PubMed: 16771844]

Jones A. A Graphics Model Building and Refinement System for Macromolecules. J Appl Cryst. 1978; 11:268–272.

Kim S, Malinverni JC, Sliz P, Silhavy TJ, Harrison SC, Kahne D. Structure and function of an essential component of the outer membrane protein assembly machine. Science. 2007; 317:961–964. [PubMed: 17702946]

Knowles TJ, Jeeves M, Bobat S, Dancea F, McClelland D, Palmer T, Overduin M, Henderson IR. Fold and function of polypeptide transport-associated domains responsible for delivering unfolded proteins to membranes. Mol Microbiol. 2008; 68:1216–1227. [PubMed: 18430136]

Konarev PV, Volkov VV, Sokolova AV, Koch MHJ, Svergun DI. PRIMUS: a Windows PC-based system for small-angle scattering data analysis. Journal of Applied Crystallography. 2003; 36:1277–1282.

Kozin MB, Svergun DI. Automated matching of high- and low-resolution structural models. Journal of Applied Crystallography. 2001; 34:33–41.

Malinverni JC, Werner J, Kim S, Sklar JG, Kahne D, Misra R, Silhavy TJ. YfiO stabilizes the YaeT complex and is essential for outer membrane protein assembly in Escherichia coli. Mol Microbiol. 2006; 61:151–164. [PubMed: 16824102]

Sanchez-Pulido L, Devos D, Genevrois S, Vicente M, Valencia A. POTRA: a conserved domain in the FtsQ family and a class of beta-barrel outer membrane proteins. Trends Biochem Sci. 2003; 28:523–526. [PubMed: 14559180]

Schuermann JP, Tanner JJ. MRSAD: using anomalous dispersion from S atoms collected at Cu Kalpha wavelength in molecular-replacement structure determination. Acta Crystal Sect D. 2003; 59:1731–1736.

Schulz GE. Transmembrane beta-barrel proteins. Adv Protein Chem. 2003; 63:47–70. [PubMed: 12629966]

Schwieters CD, Kuszewski JJ, Clore GM. Using Xplor-NIH for NMR molecular structure determination. Prog Nucl Magn Reson Spectrosc. 2006; 48:47–62.

Semenyuk AV, Svergun DI. Gnom - a Program Package for Small-Angle Scattering Data-Processing. Journal of Applied Crystallography. 1991; 24:537–540.

Sklar JG, Wu T, Gronenberg LS, Malinverni JC, Kahne D, Silhavy TJ. Lipoprotein SmpA is a component of the YaeT complex that assembles outer membrane proteins in Escherichia coli. Proc Natl Acad Sci U S A. 2007a; 104:6400–6405. [PubMed: 17404237]

Sklar JG, Wu T, Kahne D, Silhavy TJ. Defining the roles of the periplasmic chaperones SurA, Skp, and DegP in Escherichia coli. Genes Dev. 2007b; 21:2473–2484. [PubMed: 17908933]

Svergun D, Barberato C, Koch MHJ. CRYSOL - A program to evaluate x-ray solution scattering of biological macromolecules from atomic coordinates. Journal of Applied Crystallography. 1995; 28:768–773.

Svergun DI, Petoukhov MV, Koch MHJ. Determination of domain structure of proteins from X-ray solution scattering. Biophys J. 2001; 80:2946–2953. [PubMed: 11371467]

Vagin A, Teplyakov A. Molecular replacement with MOLREP. Acta Crystal Sect D. 2010; 66:22–25.

Volkov VV, Svergun DI. Uniqueness of ab initio shape determination in small-angle scattering. Journal of Applied Crystallography. 2003; 36:860–864.

Voulhoux R, Bos MP, Geurtsen J, Mols M, Tommassen J. Role of a highly conserved bacterial protein in outer membrane protein assembly. Science. 2003; 299:262–265. [PubMed: 12522254]

Voulhoux R, Tommassen J. Omp85, an evolutionarily conserved bacterial protein involved in outer-membrane-protein assembly. Res Microbiol. 2004; 155:129–135. [PubMed: 15143770]

Vranken WF, Boucher W, Stevens TJ, Fogh RH, Pajon A, Llinas M, Ulrich EL, Markley JL, Ionides J, Laue ED. The CCPN data model for NMR spectroscopy: development of a software pipeline. Proteins. 2005; 59:687–696. [PubMed: 15815974]

Ward R, Zoltner M, Beer L, El Mkami H, Henderson IR, Palmer T, Norman DG. The orientation of a tandem POTRA domain pair, of the beta-barrel assembly protein BamA, determined by PELDOR spectroscopy. Structure. 2009; 17:1187–1194. [PubMed: 19748339]

Wu T, Malinverni J, Ruiz N, Kim S, Silhavy TJ, Kahne D. Identification of a multicomponent complex required for outer membrane biogenesis in Escherichia coli. Cell. 2005; 121:235–245. [PubMed: 15851030]

Zweckstetter M, Bax A. Evaluation of uncertainty in alignment tensors obtained from dipolar couplings. J Biomol NMR. 2002; 23:127–137. [PubMed: 12153038]

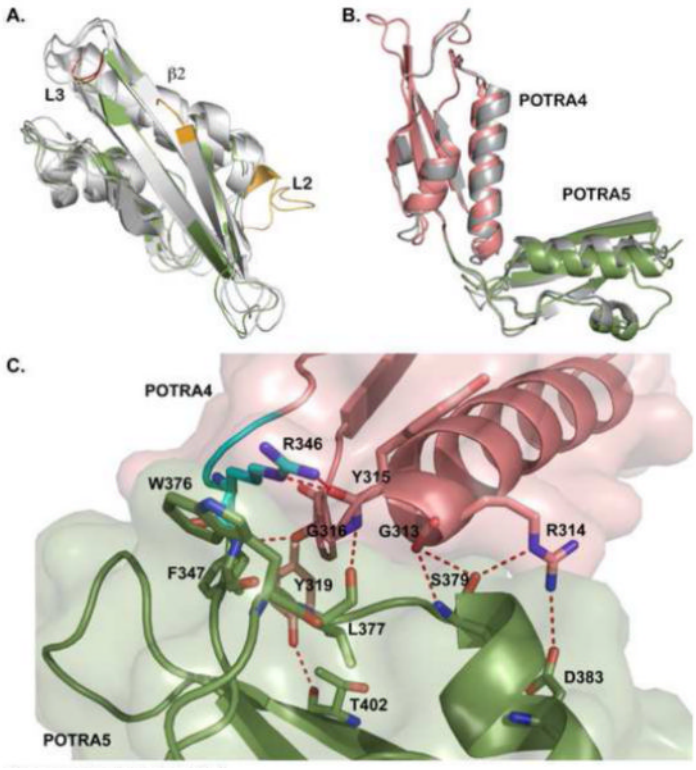

Figure 1. Crystal Structure of BamA POTRA4-5

(A) Overall structure of POTRA5 (green) and its superposition with the other four POTRA domains of BamA (grey). Unique features in POTRA3 - a 10 amino acid insertion in L2 and a β-bulge in β2, are highlighted in yellow. Three amino acid deletions in L3 in both POTRA1 and POTRA5 are highlighted in red. (B) Superposition of the two molecules in the crystallographic asymmetric unit (chains A and B). For chain A POTRA4 is shown in salmon and POTRA5 in green. Chain B is shown in gray. In both cases the POTRA4-5 fragment adopts an L-shaped conformation. (C) Interface between POTRA4 (salmon) and POTRA5 (green) shown with the Van der Waals surface semitransparent. Secondary structure elements are shown in cartoon representation, and interacting residues are shown as sticks with hydrogen bond interactions as red dotted lines. See also Table S1.

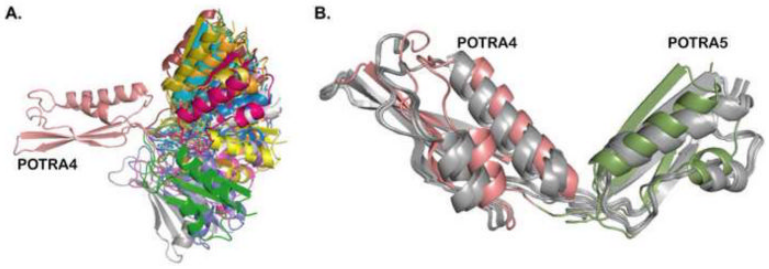

Figure 2. Solution NMR structure of BamA POTRA4-5

(A) A representative subset of the starting pool of randomized structures used to fit the experimental RDCs. POTRA4 (salmon) domains of all structures are superimposed to show the extent of structural variability in the starting pool. (B) Family of low energy NMR structures (in gray) superimposed with the X-ray structure showing good agreement between solution and crystal structures. See also Figures S1 and S2.

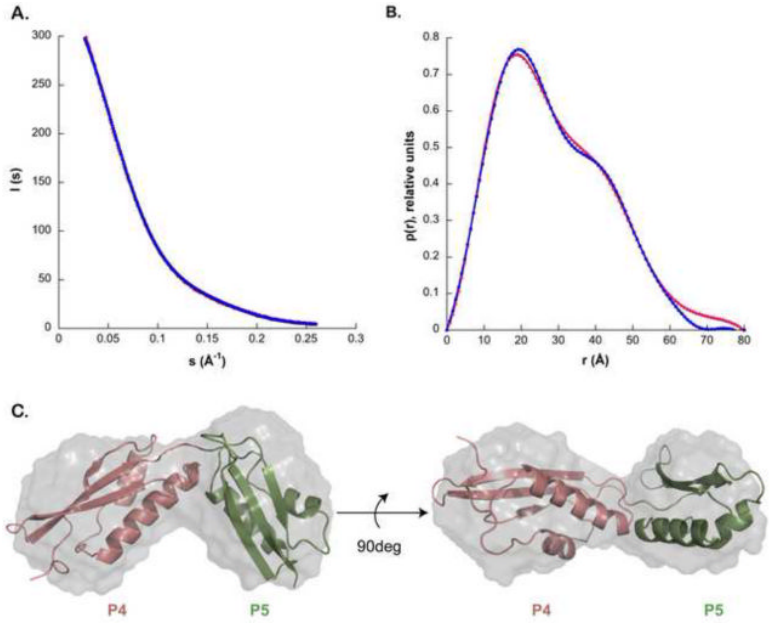

Figure 3. Solution small angle X-ray scattering structure of BamA POTRA4-5

(A) Experimental (red) and theoretical (blue) scattering curves for BamA POTRA4-5. Theoretical scattering was computed using the crystal structure coordinates for chain A of POTRA4-5. (B) Comparison of the P(r) functions calculated from the experimental (red) and coordinate-derived (blue) scattering curves for BamA POTRA4-5. (C) Two views, related by a 90° rotation, of the averaged *ab initio* reconstruction of the BamA POTRA4-5 molecular envelope calculated by GASBOR from the SAXS data (semitransparent gray surface) superimposed on the crystal structure of POTRA4-5 (cartoon representation, POTRA4-salmon, POTRA5-green). See also Figure S3A.

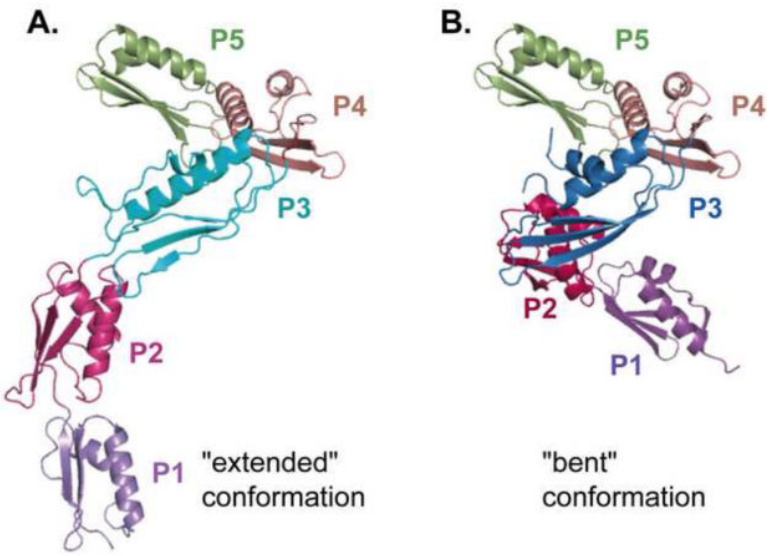

Figure 4. Spliced models of the complete periplasmic domain of BamA

Spliced models for the “extended” (A) and “bent (B) conformations of the BamA periplasmic domain generated by superimposing POTRA4 from in the POTRA4-5 fragment with POTRA4 in the POTRA1-4 structures PDB ID: 3EFC (Gatzeva-Topalova et al., 2008) and PDB ID: 2QCZ (Kim et al., 2007) respectively.

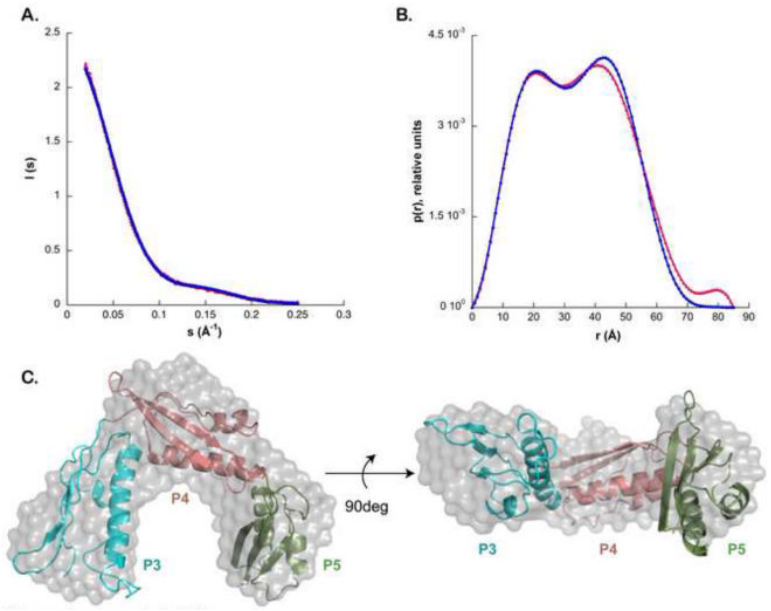

Figure 5. Solution small angle X-ray scattering structure of BamA POTRA3-5

(A) Experimental (red) and theoretical scattering curves for BamA POTRA3-5. Theoretical scattering was computed using the spliced model for POTRA3-5. (B) Comparison of the P(r) functions calculated from the experimental (red) and theoretical (blue) scattering curves for the BamA POTRA3-5 fragment. (C) Two views, related by a 90° rotation, of the averaged *ab initio* reconstruction of the BamA POTRA3-5 molecular envelope calculated by GASBOR from the SAXS data (semitransparent gray surface) superimposed on the spliced model of POTRA3-5 (cartoon representation). See also Figure S3B.

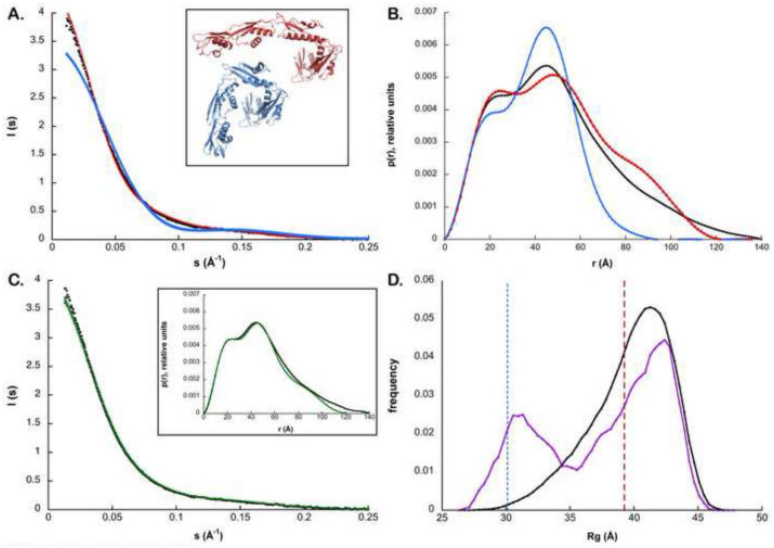

Figure 6. SAXS analysis of the periplasmic domain of BamA (POTRA1-5)

(A) Comparison of experimental (black) and theoretical scattering curves of POTRA1-5. Theoretical scattering curves were calculated based on the "extended" (inset, red) and "bent" (inset, blue) spliced models of BamA periplasmic domain. (B) Comparison of the P(r) functions calculated from the experimental scattering curve (black), the "extended" model (red) and the "bent" model (blue). None of the spliced models fully represents the solution structure of the BamA periplasmic domain. (C) Experimental scattering curve (black) compared to a theoretical scattering curve (green) computed from a "mixture" of the extended and bent conformations (present at 74% and 26% respectively). The inset shows the P(r) functions calculated from the experimental (black) and theoretical (green) scattering curves. (D) R_g distributions for the initial pool of 10,000 randomized structures of POTRA1-5 used in the Ensemble Optimization Method (black), and the selected optimized ensemble of conformations (purple). The two vertical dashed lines represent the R_g values calculated from the "bent" (blue) and "extended" (red) spliced models of BamA periplasmic domain. See also Figure S3C.

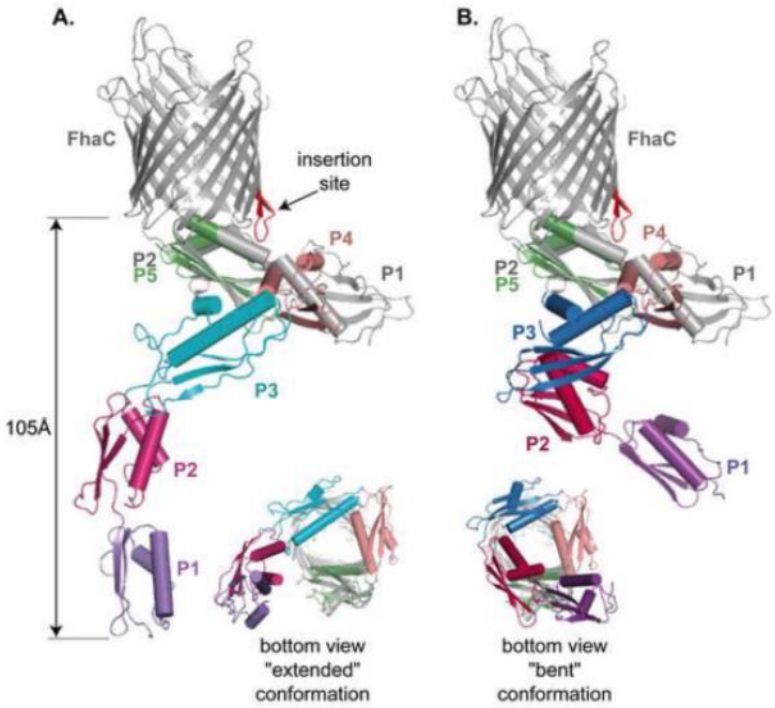

Figure 7. BamA and FhaC structure superpositions

(A) Side and bottom view of FhaC superimposed on the extended conformation of BamA. POTRA5 from the periplasmic domain of BamA in the “extended” conformation was superimposed on POTRA2 of FhaC (in grey). (B) Side and bottom view of FhaC superimposed on the bent conformation of BamA. POTRA5 from the periplasmic domain of BamA in the “bent” conformation superimposed on POTRA2 of FhaC (in grey). The POTRA1 domain of FhaC is removed from the bottom views for clarity.

Table 1

Data collection, phasing and refinement statistics

	Se-Met BamA$_{264-424}$
Data collection	
Space group	$P3_221$
Cell dimensions:	
a=*b* (Å)	118.49
c (Å)	69.99
α=β (°)	90
γ (°)	120
Wavelength	0.9798
Resolution (Å)[a]	40.00-2.70
	(2.80-2.70)
R_{sym} [b]	8.4 (24.2)
$I / \sigma I$	8.4 (2.6)
Completeness (%)	96.8 (97.3)
Redundancy	1.5 (1.4)
Phasing	
FOM before DM[c]	0.27
FOM after DM	0.68
Refinement	
Resolution (Å)	38.79-2.69
	(2.79-2.69)
No. reflections	28,390
No. atoms	2,357
R_{work} [d]	21.2 (26.6)
R_{free}	26.0 (28.7)
Mean *B*-factor all atoms, chain A	29.1
Mean *B*-factor all atoms, chain B	60.0
Mean *B*-factor, solvent	31.4
RMS deviation from ideal values:	
bond lenghts (Å)	0.009
bond angles (°)	1.2
Ramachandran, residues in:	
most favored region (%)	89.4
allowed regions (%)	10.6

[a] Values in parentheses are for highest-resolution shell.

[b] $R_{sym}=\Sigma_h\Sigma_i|(I_i(h)-< I(h)>|/ \Sigma_h\Sigma_I I_i(h)$, where $I_i(h)$ is the I-th measurement of reflection h, and <I(h)> is the weighted mean of all measurements of h.

[c] FOM=Figure Of Merit; DM=Density Modification

[d] $R_{work} = \Sigma|F_{obs}-F_{calc}|/\Sigma F_{obs}$ where F_{obs}=observed structure factor amplitude and F_{calc} = structure factor calculated from model. R_{free} is computed in the same manner as R_{work}, using the test set of reflections.